# DUST EMISSION FROM ACTIVE GALACTIC NUCLEI

Maia Nenkova<sup>1</sup>, Željko Ivezić<sup>2</sup> and Moshe Elitzur<sup>1</sup>

maia@pa.uky.edu, ivezic@astro.princeton.edu, moshe@pa.uky.edu

### ABSTRACT

Unified schemes of active galactic nuclei (AGN) require an obscuring dusty torus around the central source, giving rise to Seyfert 1 line spectrum for pole-on viewing and Seyfert 2 characteristics in edge-on sources. Although the observed IR is in broad agreement with this scheme, the behavior of the 10  $\mu$ m silicate feature and the width of the far-IR emission peak remained serious problems in all previous modeling efforts. We show that these problems find a natural explanation if the dust is contained in  $\sim 5$ –10 clouds along radial rays through the torus. The spectral energy distributions (SED) of both type 1 and type 2 sources are properly reproduced from different viewpoints of the same object if the optical depth at visual of each cloud obeys  $\tau_{\rm V} \gtrsim 60$  and the clouds' mean free path increases roughly in proportion to radial distance.

Subject headings: dust: extinction—galaxies: active—galaxies: nuclei—galaxies: Seyfert—quasars: general—radiative transfer

## 1. INTRODUCTION

Although there is a bewildering array of AGN classes, a unified scheme has been emerging steadily (e.g. Antonucci 1993, 2002; Wills 1999). The nuclear activity is powered by a supermassive ( $\sim 10^6-10^9~M_{\odot}$ ) black hole and its accretion disk, which extends to  $\sim 1~{\rm pc}$ . This central engine is surrounded by a dusty toroidal structure, extending to  $\gtrsim 100~{\rm pc}$ . Much of the observed diversity is simply the result of viewing this axisymmetric geometry from different angles. The torus provides anisotropic obscuration of the central region so

 $<sup>^{1}</sup>$ Department of Physics and Astronomy, University of Kentucky, Lexington, KY 40506–0055

<sup>&</sup>lt;sup>2</sup>Department of Astrophysical Sciences, Princeton University, Princeton, NJ 08544

that sources viewed face-on are recognized as Seyfert 1 galaxies, those observed edge-on are Seyfert 2. The primary evidence for the torus comes from spectropolarimetric observations of type 2 sources, which reveal hidden type 1 emission via reflection off material situated above the torus opening. While compelling, this evidence is only indirect in that it involves obscuration, not direct emission by the torus itself.

An obscuring dusty torus should reradiate in IR the fraction of nuclear luminosity it absorbs, providing direct evidence for its existence. Indeed, the continua from most AGN show significant IR emission. Silicates, whose presence is revealed by a spectral feature at 10  $\mu$ m, are a major constituent of astronomical dust. Seyfert 2 sources display this feature in absorption—as expected for edge-on viewing of an optically thick torus. However, contrary to expectations for face-on viewing, quasars and Seyfert 1 galaxies do not show this feature in emission, (Roche et al 1991; recent claims by Clavel et al 2000 notwithstanding). This poses a serious problem to models of the dusty torus emission, which must suppress the silicate feature in type 1 objects while producing it in type 2. Laor and Draine (1993) studied the effects of altering the dust properties and conclude that suppression of the 10  $\mu$ m feature requires significant silicate depletion or very large (up to 10  $\mu$ m) grains (see also Maiolino et al 2001). This could explain type 1 SED but would require a different explanation for type 2 objects with their prominent 10  $\mu$ m absorption feature.

Pier & Krolik (1992, 1993) were the first to explore the effects of toroidal geometry on dust radiative transfer. They note that the AGN dust must be in clumps to protect the grains, but because of the difficulties in modeling a clumpy distribution they approximate it with a uniform one instead. They also neglect scattering. In spite of these approximations, their results are encouraging. The directional dependence of their model radiation reproduces the gross features of observed SED, indicating that the toroidal geometry captures the essence of IR observations. Two major problems remain: the observed emission has a far-IR peak much broader than the models can produce, and the silicate emission feature is suppressed in faceon viewing only in a narrow, finely-tuned range of the model parameters. Rowan-Robinson (1995) notes that both problems could be alleviated by clumpiness. He argues that a spherical shell is an adequate proxy for a clump, and produces type 1 IR emission from a superposition of such concentric shells. But the shell/clump analogy is fundamentally problematic: Since the illuminated and dark faces of a clump produce widely different spectra, the observed SED varies with the angle between radiation source, clump and observer (see fig. 1). In contrast, outside an optically thick spherical shell the SED is always the same irrespective of observer location because only the dark side is ever visible (inside the shell, only the illuminated face is visible). Concentric spherical shells cannot substitute for clumps.

We performed a more adequate calculation of IR emission from an obscuring clumpy

torus, combining realistic modeling of the emission from externally illuminated clumps with proper handling of cloud shadowing. The latter is an essential ingredient since the number of clouds along radial rays through the torus must be sufficiently large to ensure that x-rays from the central engine are virtually always attenuated in type 2 objects (Guainazzi et al 2001). Here we report the results of our effort, which show that the SED of both type 1 and type 2 objects are properly reproduced at different viewing angles of the same clumpy torus—in agreement with unified schemes. In a forthcoming publication we will provide a more detailed account of our calculations and the results.

## 2. EMISSION FROM A CLUMPY MEDIUM

Consider a medium where the dust is in clouds. For simplicity, each cloud has the same optical depth  $\tau_{\lambda}$ . Along a given path, the mean number of clouds encountered in segment ds is  $d\mathcal{N}(s) = ds/\ell(s)$ , where  $\ell = (n_c A_c)^{-1}$  is the mean free path between clouds  $(A_c)$  is the cloud area perpendicular to the path and  $n_c$  is the number density of clouds). As long as  $\ell \gg R_c$ , where  $R_c$  is the cloud radius, each cloud can be considered a point source of intensity  $S_{c\lambda}$ , and the intensity generated along the segment is  $S_{c\lambda}d\mathcal{N}$ . Denote by  $P_{\rm esc}$  the probability that this radiation propagate along the rest of the path without absorption by any other cloud. Natta & Panagia (1984) show that Poisson statistics for the distribution of clumps yields

$$P_{\rm esc} = e^{-t_{\lambda}}, \quad \text{where} \quad t_{\lambda} = \mathcal{N}(s)(1 - e^{-\tau_{\lambda}})$$
 (1)

and  $\mathcal{N}(s) = \int_s d\mathcal{N}$  is the mean number of clouds along the rest of the path. The contribution of segment ds to the emerging intensity is simply  $P_{\rm esc}S_{\rm c\lambda}d\mathcal{N}$  and the flux from the cloud distribution at distance D is

$$F_{\lambda}^{C} = \frac{1}{D^{2}} \int dA \int e^{-t_{\lambda}} S_{c\lambda}(s) d\mathcal{N}(s)$$
 (2)

where dA is the surface area element perpendicular to the line of sight. Given the geometry, the flux can be calculated from this expression once  $S_{c\lambda}$  is known.

Clouds are heated by radiation from both the AGN and all other clouds. Consider first the direct heating by the AGN (figure 1). Since our interest is in optically thick clouds only, the dust temperature is much higher on the illuminated face than any other part of the surface. Therefore the cloud emission varies strongly with direction, and the corresponding source function  $S_{c\lambda}^{d}(r,\alpha)$  depends on both distance r and position angle  $\alpha$ . The clump shape is of course arbitrary, and we have constructed "synthetic clumps" by averaging the emission from an illuminated slab over all possible slab orientations. This procedure utilizes an exact

solution of radiative transfer for external illumination and also reproduces the  $\alpha$ -dependence of the observed fraction of illuminated area on the surface of a spherical-like object.

We conducted detailed calculations with the code DUSTY (Ivezić, Nenkova & Elitzur 1999). The code preforms an exact solution of the slab radiative transfer problem including dust absorption, emission and scattering. The optical depth across the slab thickness at wavelength  $\lambda$  is  $\tau_{\lambda} = q_{\lambda}\tau_{V}$  where  $\tau_{V}$  is the optical depth at visual and  $q_{\lambda}$  is the proper efficiency factor of standard interstellar dust. With AGN luminosity  $L_{12} = L/10^{12}L_{\odot}$ , the illuminating bolometric flux is  $F_{e} = L/4\pi r^{2}$ . Its spectral shape, typical for AGN, is  $\lambda f_{\lambda}$  = constant in the wavelength range 0.01–0.1  $\mu$ m and  $\propto \lambda^{-0.5}$  for 0.1–100  $\mu$ m (cf Pier & Krolik 92, Laor & Draine 93). For any slab orientation, the solution of the radiative transfer problem determines the temperature run in the slab and the intensity it emits toward any direction. Therefore the dust temperature  $T_{\rm n}$  on the illuminated face of a slab normal to the radius vector can replace the external flux  $F_{e}$  as a specifier of location.

The top panel of figure 2 shows typical results for  $S_{\rm c\lambda}^{\rm d}$ . The clump spectrum was constructed by averaging over all slab orientations the solutions for slabs with  $\tau_{\rm V}=100$  at radial distances where  $T_{\rm n}=800$  K (corresponding to  $r=4\,L_{12}^{1/2}$  pc). The 10  $\mu{\rm m}$  silicate feature is seen in absorption at small  $\alpha$ , switching to increasingly more pronounced emission as  $\alpha$  increases and a larger fraction of the clump illuminated face becomes visible.

An exact calculation of the effects of diffuse radiation from all clouds is a formidable task, akin to a full solution of the radiative transfer problem in which individual dust particles themselves are dusty clouds. However, compared with the AGN radiation, heating by the diffuse radiation is highly inefficient because it involves long wavelengths, and thus can be neglected. Emission from clouds with direct view of the AGN is well described by  $S_{c\lambda}^d$ . But clouds whose line-of-sight to the AGN is blocked by another cloud will be heated only indirectly by the diffuse radiation. We approximate the diffuse radiation field at r by angle-averaging over  $\alpha$  the emission  $S_{c\lambda}^d(r,\alpha)$  from clouds directly heated by the AGN. In this radiation field we imbed a sphere with constant density profile and solve for its temperature and emission. Our approximation for the source function of indirectly illuminated clouds is  $S_{c\lambda}^i = F/\Omega$ , where F is the flux and  $\Omega$  the solid angle of such a sphere at a large distance. The bottom panel of figure 2 shows a sample of  $S_{c\lambda}^i$ , together with the corresponding source functions for direct heating.

At distance r the probability for unhindered view of the AGN is  $p(r) = e^{-\mathcal{N}(r)}$ , where  $\mathcal{N}(r) = \int_{-\infty}^{r} dr/\ell$  is the mean number of clouds to the AGN. Our approximation for the clump source function is

$$S_{c\lambda} = p S_{c\lambda}^{d} + (1 - p) S_{c\lambda}^{i}.$$

$$(3)$$

The steps we outlined can be iterated to become an exact solution scheme for radiative transfer in clumpy medium. The small magnitude at short wavelengths, which control heating, of  $S_{c\lambda}^i/S_{c\lambda}^d$  evident in figure 2 indicates that this process should converge rapidly. Eq. 3 is equivalent to its first two steps.

### 3. MODEL RESULTS

We model the AGN obscuring region as a toroidal distribution of dusty clouds, shown in figure 1. Instead of the inner radius  $R_{\rm i}$  we specify as input  $T_{\rm ni} = T_{\rm n}(R_{\rm i})$ , the surface temperature of a normally illuminated slab at  $R_{\rm i}$ . In all calculations we set  $T_{\rm ni} = 1400$  K, the temperature below which both silicate and graphite grains exist; this choice implies  $R_{\rm i} = 1.2\,L_{12}^{1/2}$  pc for a  $\tau_{\rm V} = 100$  cloud. The geometry requires two additional input parameters: The torus thickness  $Y = R_{\rm o}/R_{\rm i}$ , equivalent to the lowest  $T_{\rm n}$  in the torus, and  $\Theta$ , the conical opening half-angle. Assuming power law variation for the mean free path  $\ell \propto r^q$ , the cloud distribution is described by the two input parameters q and  $\mathcal{N}_{\rm T} = \int_{R_{\rm i}}^{R_{\rm o}} dr/\ell$ , the number of clouds along a radial ray through the torus. The final free parameter is  $\tau_{\rm V}$ , the optical depth of each cloud. The grain efficiency factor  $q_{\lambda}$  and the AGN spectral shape  $f_{\lambda}$  are set to their standard values. The observed flux is determined from

$$F_{\lambda} = \frac{L}{4\pi D^2} f_{\lambda} e^{-t_{\lambda T}} + F_{\lambda}^{C} \tag{4}$$

where  $F_{\lambda}^{\rm C}$  is calculated from eq. 2 and  $t_{\lambda \rm T}$  from eq. 1 with  $\mathcal{N}(s) = \mathcal{N}_{\rm T}$  for type 2 sources and zero for type 1. Extracting the overall bolometric flux  $F_{\rm B} = L/4\pi D^2$ , the SED is controlled by  $T_{\rm n\,i}$  and five dimensionless free parameters: Y and  $\Theta$  specify the geometry,  $\tau_{\rm V}$  the individual clouds and  $\mathcal{N}_{\rm T}$  and q the cloud distribution.

We performed extensive calculations and find a large range of the free parameters that yield satisfactory agreement with observations. A detailed report of our results will be provided elsewhere, here we show in figure 3 a representative model. Our aim is to reproduce the typical SED of the type 1 and type 2 families, not to fit in detail any particular object. Data points for type 1 sources show average spectra for radio-quiet quasars (Sanders et al 1989, Elvis et al 1994) and Seyfert 1 galaxies (Granato & Danese 1994). Because of the high obscuration of the AGN in type 2 sources, fluxes for their nuclear regions properly extracted out of the contributions of the host galaxy and starburst regions are scarce. We show data for reliable measurements of four individual objects. The data were scaled for a rough match of the model results without attempting a best fit. Detailed fitting of type 2 objects, when warranted, will determine their bolometric flux  $F_{\rm B}$ , a quantity inaccessible for direct measurement because the bulk of the flux is emitted away from Earth.

Our models reproduce the broad IR bump extending to  $\sim 100~\mu\text{m}$ , as observed. Furthermore, the 10  $\mu\text{m}$  feature appears in absorption in equatorial viewing but is smeared out in axial viewing in spite of its prominence in emission from directly-heated individual clouds (fig. 2). The reason is that most of these clouds are blocked from view even along the axis. We find satisfactory results for conical opening  $\Theta = 45 \pm 15^{\circ}$ . The torus thickness can vary in the range Y = 50–250, i.e.,  $R_{\rm o}/L_{12}^{1/2} = 60$ –300 pc. At smaller Y the IR bump is not broad enough, larger Y produce too much 20–100 $\mu$ m emission. The number of clouds is  $\mathcal{N}_{\rm T} = 5$ –10. When  $\mathcal{N}_{\rm T} < 5$  the  $10\mu$ m feature appears in emission in pole-on spectra,  $\mathcal{N}_{\rm T} > 10$  shifts the spectrum to longer wavelengths resulting in too little 1–10 $\mu$ m emission and too much 20–100 $\mu$ m. The power index should be  $q = 1 \pm 0.5$ . At larger q the far-IR bump is not high enough, as is evident in figure 3, at smaller q it is too high.

Significantly, the only constraint on the optical depth of individual clouds is  $\tau_{\rm V} \gtrsim 60$ . The results vary only slightly when  $\tau_{\rm V}$  increases from 60 to 100, and hardly at all during further increase. The reason is simple. The dependence on  $\tau_{\rm V}$  arises from the probability for photon escape and the cloud source function. From eq. 1,  $P_{\rm esc} = e^{-\mathcal{N}}$  whenever  $\tau_{\lambda} \gg 1$ , and at  $\tau_{\rm V} \gtrsim 60$  this condition is met at all relevant wavelengths. Similarly, because the clouds are heated externally, only their surface is heated significantly when  $\tau_{\rm V}$  is large. Increasing  $\tau_{\rm V}$  further only adds cool material, thus  $S_{\rm c\lambda}$  saturates for all relevant  $\lambda$ , similar to standard black-body emission. Extending our calculations all the way to  $\tau_{\rm V} = 500$ , we have verified that increasing  $\tau_{\rm V}$  indeed has no effect on the model results.

## 4. DISCUSSION

The cloud distribution is described by q and  $\mathcal{N}_{\rm T}$ , individual clouds by the optical depth  $\tau_{\rm V}$ . No other cloud property was specified. The cloud size enters only indirectly through the underlying assumption  $R_c \ll \ell$ . If  $V_c \simeq A_c R_c$  is the volume of a single cloud, the volume filling factor of the cloud population is  $\phi = n_c V_c = R_c/\ell$ . Our calculations apply to small filling factors,  $\phi \ll 1$ , the Pier & Krolik model involves the opposite limit  $\phi = 1$ . The mean free path scale can be determined from  $\ell(R_i)/R_i = (1/\mathcal{N}_{\rm T}) \int_1^Y y^{-q} dy$ . The model with q = 1,  $\mathcal{N}_{\rm T} = 5$  and Y = 100 has  $\ell(R_i) = 0.9 R_i = 1.1 L_{12}^{1/2}$  pc. A reasonable realization of this model, though not unique, is a constant  $\phi = 0.1$  throughout the torus so that  $R_c = 0.09 r$ . When  $\tau_{\rm V} = 100$  and  $L_{12} = 1$ , the clouds vary from  $R_c \sim 0.1$  pc with gas density  $\sim 3 \, 10^5$  cm<sup>-3</sup> in the torus inner regions to  $R_c \sim 10$  pc with density  $\sim 3 \, 10^3$  cm<sup>-3</sup> at the outer edge. The torus could contain additional clouds with smaller  $\tau_{\rm V}$  without significantly affecting the SED.

The properties we deduce for the torus agree with independent estimates. Based on 88

Seyfert galaxies Schmitt et al (2001) conclude that  $\Theta=48^{\circ}$ , at the center of the range we find. Our minimal cloud number  $\mathcal{N}_{\rm T}=5$  implies a probability  $\leq e^{-5}=710^{-3}$  for unattenuated view of the AGN in type 2 sources, in agreement with the findings of Guainazzi et al (2001). From x-ray measurements of 73 Seyfert 2 galaxies Bassani et al (1999) find a large variation in column density, with a mean of  $3\,10^{23}$  cm<sup>-2</sup> and  $\gtrsim 10^{24}$  cm<sup>-2</sup> for as many as a third of the sources. The mean is comparable with the column density of our torus for 5 clouds of  $\tau_{\rm V}\gtrsim 60$  each and standard dust-to-gas ratio. Furthermore, the similarity of SED among type 2 sources in spite of the large x-rays column variation is a natural consequence of our model:  $\tau_{\rm V}$  is bounded only from below, the SED remains the same at all  $\lambda\gtrsim 1\mu{\rm m}$  for arbitrary increase in overall column. But x-ray absorption does vary with the latter because the optical depth for Thompson scattering is only  $\sim 10^{-2}\tau_{\rm V}$ . Sources with small columns may show up in x-ray absorption while selectively excluded from IR observations because of their weak emission.

Our results add strong support for unification schemes of AGN. In accordance with such schemes, the IR emission from both type 1 and type 2 sources is reproduced at different viewing of the same geometry when proper account is taken of the torus clumpiness.

We have greatly benefitted from discussions with many colleagues, especially J. Conway, A. Laor, N. Levenson and H. Netzer. Support by NASA and NSF is gratefully acknowledged.

#### REFERENCES

Antonucci, R., 1993, ARA&A, 31, 473

Antonucci, R., 2002, in Astrophysical Spectropolarimetry, ed. J. Trujillo-Bueno, F. Moreno-Insertis & F. Sanchez (Cambridge University Press), 151

Bassani L., et al 1999, ApJS, 121, 473

Clavel, J. et al., 2000, A&A, 357, 839

Draine, B.T., & Lee, H.M., 1984, ApJ, 285, 89

Dudley, C.C., & Winn-Williams, C.G., 1997, ApJ, 488, 720

Elvis, M. et al., 1994, ApJS, 95, 1

Granato, G.L. & Danese, L., 1994, MNRAS, 268, 235

Guainazzi, M., Fiore, F., Matt, G. & Perola, G. C., 2001, MNRAS, 327, 323

Imanishi, M., & Ueno, S., 2000, ApJ, 535, 626

Ivezić,Ž., Nenkova, M. & Elitzur, M. 1999, User Manual for DUSTY, Univ. of Kentucky Internal Report<sup>3</sup>

Laor, A., & Draine, B.T., 1993, ApJ, 402, 441

Maiolino, R. et al., 2001, A&A, 365, 28

Natta, A. & Panagia, N., 1984, ApJ, 287, 228

Pier, E., & Krolik, J., 1992, ApJ, 401, 99

Pier, E., & Krolik, J., 1993, ApJ, 418, 673

Rieke, G. & Low, F. 1975, ApJ, 199, L13

Roche, P. et al., 1991, MNRAS 248, 606

Rowan-Robinson, M., 1995, MNRAS 272, 737

Sanders, D. et al., 1989, ApJ, 347, 29

Schmitt H.R., et al, 2001, ApJ, 555, 663

Wills, B. J. 1999, in ASP Conf. Ser. 162, Quasars and Cosmology, ed. G. Ferland & J. Baldwin (San Francisco: ASP), 101

 $<sup>^3</sup>$ accessible at http://www.pa.uky.edu/ $\sim$ moshe/dusty/

This preprint was prepared with the AAS IATEX macros v5.0.

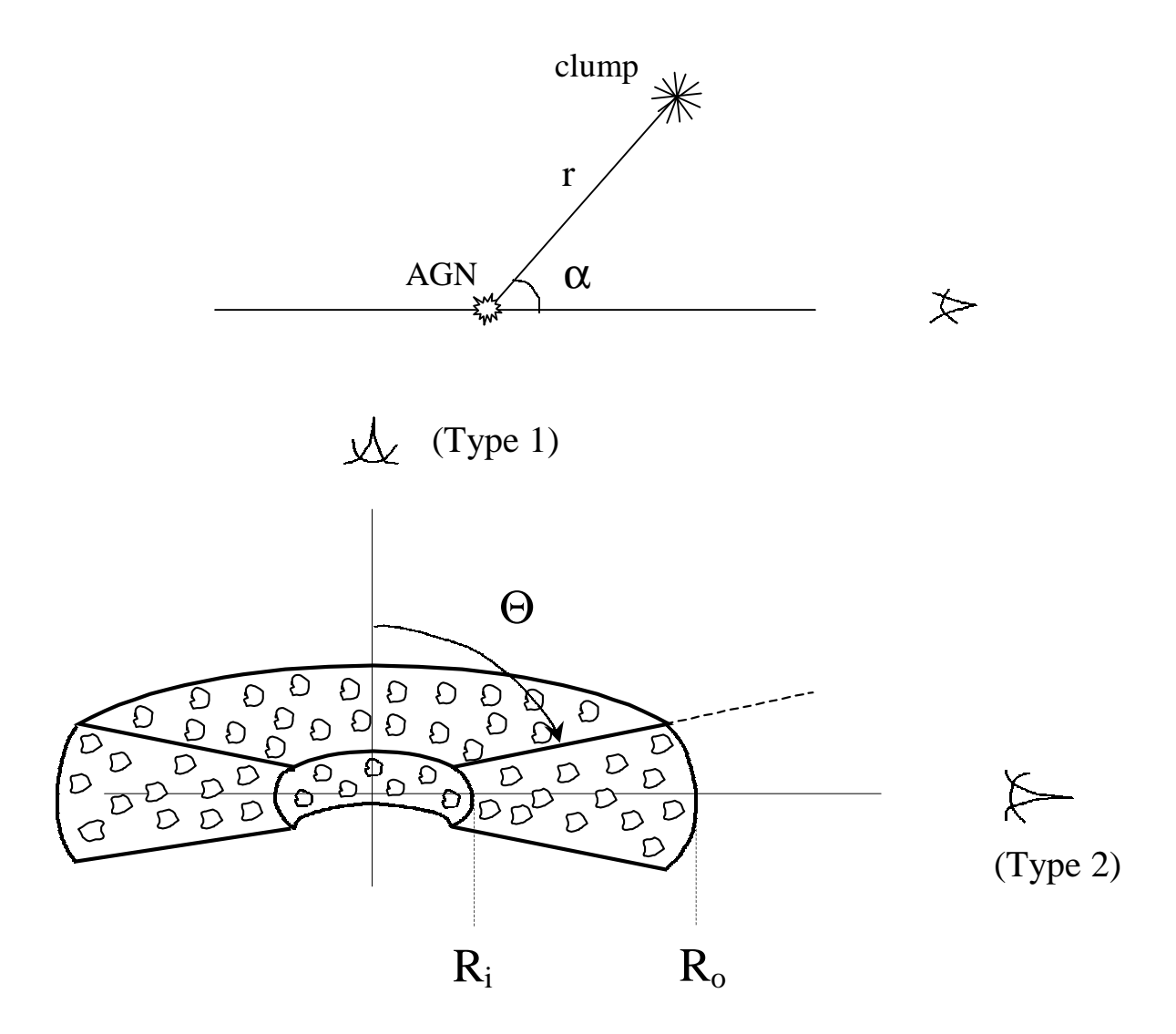


Fig. 1.— Model geometry. Top: Positions of the AGN, clump and observer. As the position angle  $\alpha$  varies at fixed distance r, the visible fraction of the clump's illuminated area changes and with it the observed radiation. Bottom: The clumpy torus.

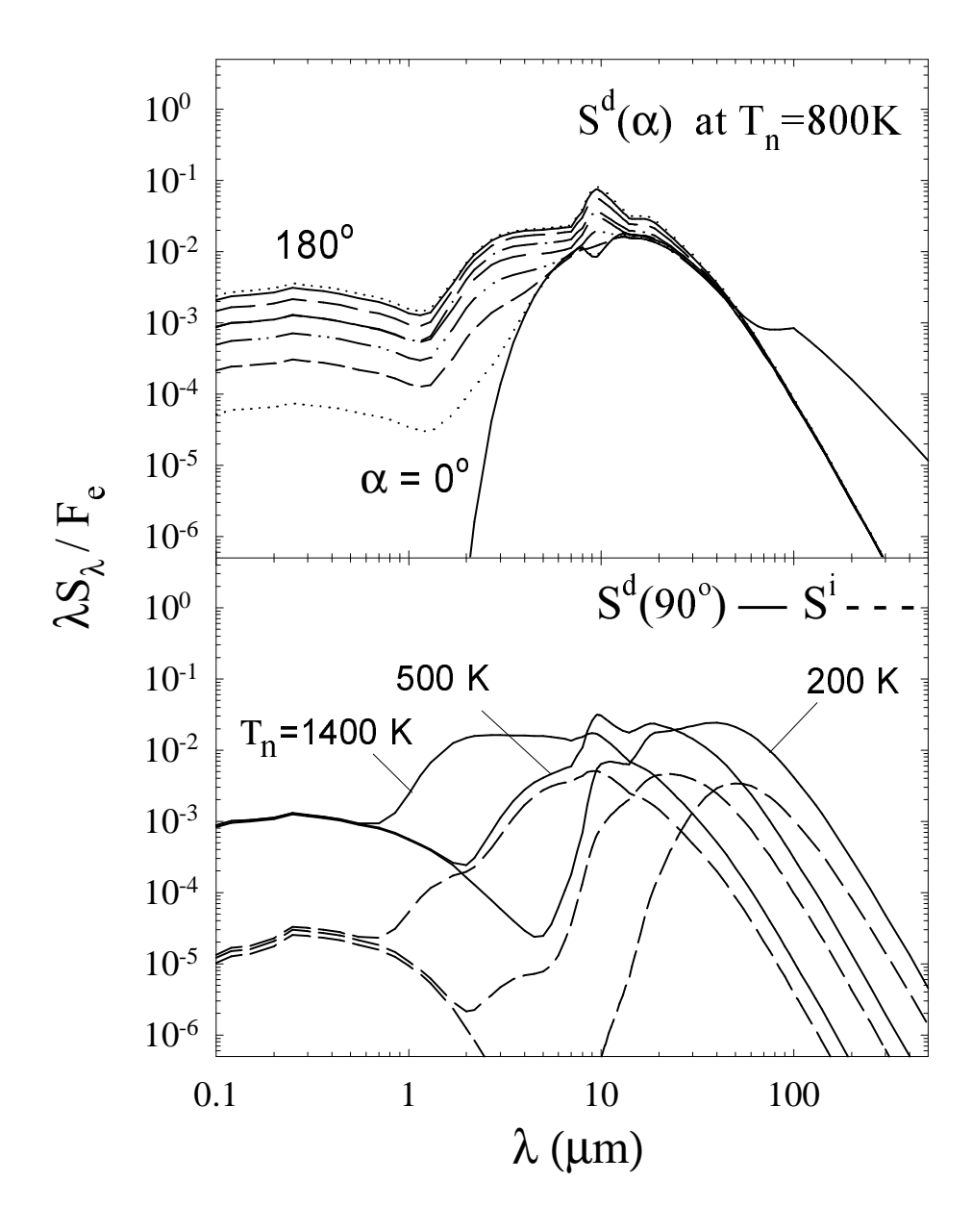


Fig. 2.— Emission from  $\tau_{\rm V}=100$  clumps normalized to the AGN local bolometric flux  $F_e=L/4\pi r^2$ . Top: The source  $S_{\rm c\lambda}^{\rm d}$  for directly heated clouds at distance where  $T_{\rm n}=800~{\rm K}$  ( $r=4L_{12}^{1/2}$  pc for this  $\tau_{\rm V}$ ). The position angle  $\alpha$  is shown at 22.5° intervals. Bottom: Emission of directly ( $S_{\rm c\lambda}^{\rm d}$ , full lines) and indirectly ( $S_{\rm c\lambda}^{\rm i}$ , dashed lines) heated clouds at distances where  $T_{\rm n}=1400,\,500$  and 200K, or  $r/L_{12}^{1/2}=1,\,10,\,100$  pc, respectively. The source function for direct heating is shown at  $\alpha=90$ .

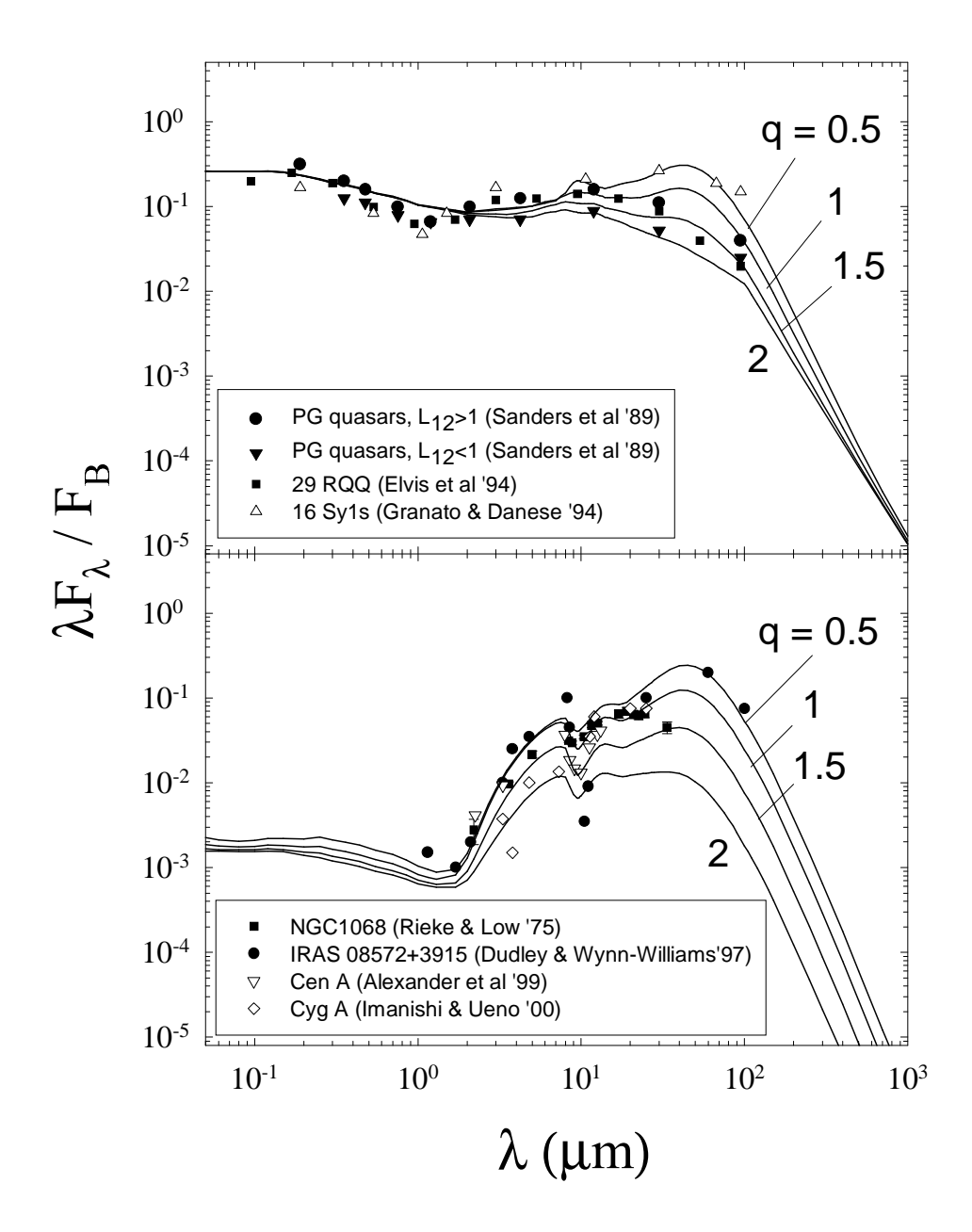


Fig. 3.— Modeling and observations of type 1 (top panel) and type 2 (bottom) sources. Lines are model results for the axial and equatorial views of the clumpy torus shown in figure 1, with  $F_{\rm B}=L/4\pi D^2$ . Radial rays through the torus have 5 clouds on average, each with  $\tau_{\rm V}=100$ . The clouds' mean free path varies as  $r^q$ , with the indicated q. The torus inner radius corresponds to temperature  $T_{\rm n\,i}=1400~{\rm K}~(R_{\rm i}=1.2\,L_{12}^{1/2}~{\rm pc})$  and it has  $R_{\rm o}=100R_{\rm i}$  and  $\Theta=45^{\circ}$ . Data for type 1 are composite spectra from the indicated compilations, type 2 are for individual objects. Each data set was scaled for rough matching with the models.